

Torsional deformation properties of SMA tapes and their application to bias-type reciprocating rotary driving actuator

K. TAKEDA¹⁾, R. MATSUI¹⁾, H. TOBUSHI¹⁾, E. A. PIECZYSKA²⁾

¹⁾*Department of Mechanical Engineering
Aichi Institute of Technology
1247 Yachigusa, Yakusa-cho, Totota 470-0392, Japan
e-mail: k-takeda@aitech.ac.jp*

²⁾*Institute of Fundamental Technological Research
Polish Academy of Sciences
Pawińskiego 5b
02-106 Warsaw, Poland*

IN ORDER TO DEVELOP THE RECIPROCATING rotary driving actuator with a simple mechanism using shape memory alloy (SMA) tapes, the graphical method to design the actuator was proposed based on the torsional deformation properties of SMA tapes. The torsional deformation properties of the SME tape showing the shape memory effect (SME) and the SE tape showing superelasticity (SE) were obtained. The bias-type reciprocating rotary actuator was composed of the pretwisted SME tape and the flat SE tape in series. The design chart expressed by the relationship between torque and twisting angle of the SME tape and the SE tape was proposed. The rotational angle and torque, which vary depending on temperature, can be estimated based on the design chart. The rotational angle is controlled by adjusting the mounting angle of the SME tape and the heating temperature. The automatically opening and closing blind driven by sunlight was demonstrated. The blind was controlled by using the reciprocating rotary element composed of the SME tape and the SE tape. The behavior of the blind can be achieved based on the proposed design method of the reciprocating rotary driving element.

Key words: shape memory alloy, tape, torsion, actuator, reciprocating rotation, design chart, bias-type.

Copyright © 2017 by IPPT PAN

1. Introduction

ONE OF THE MAIN MATERIALS which have prompted research on smart materials and structures is a shape memory alloy (SMA). The main characteristics of SMAs are the shape memory effect (SME) and superelasticity (SE) [1–4]. SMAs are used in the driving elements of actuators, robots and heat engines by applying these characteristics. TiNi SMAs are most widely used in practical applications due to their high performance with respect to recovery strain, re-

covery stress, cyclic deformation property, fatigue strength, corrosion resistance and wear resistance.

The SME and SE appear based on martensitic transformation (MT). The deformation properties of SME and SE depend highly on temperature and stress. In a recent study using the torsional deformation of a TiNi SMA tube, a twist in the blades of rotor aircraft was investigated in order to improve the flight performance [5, 6]. Thin wires and thin tapes are widely used in practical applications because of the adaptable thermal response of SMA elements. In addition, in practical applications, when SMA thin tapes are used, torsional deformation can be obtained by twisting the SMA tape by simply holding both ends with simple flat grippers and without any machining of the SMA tape [7, 8]. If the characteristics of the SE with high plateau stress are applied to torsional deformation of SMA tapes, a high performance of energy storage can be achieved similar to that of a torsion bar. In this way, i.e., by using the torsional characteristics of SMA thin tapes, simple and small actuators can be developed [9, 10].

In applications of SMA actuators, the two-way displacement is widely obtained through temperature variation [11, 12]. The deformation to the deformed direction during cooling is necessary for the two-way motion. Some internal stress in the parent phase of SMAs is required to induce the two-way property. The internal stress cannot be controlled easily in SMAs; therefore the required two-way characteristics are difficult to attain. In order to obtain the two-way motion, the so-called “bias” technique is widely used [13–19]. In the typical bias-type actuators, a one-way SMA is combined with itself or other component. The SMA has high stiffness and high plateau stress at high temperature, and low stiffness and low plateau stress at low temperature. The SMA component is deformed by the higher force in the bias component at low temperature and moves to its original shape by the recovery force induced in the SMA component at high temperature. The two-way actuation is achieved since the SMA component will be deformed again when the temperature falls. There are various advantages in the bias-type actuator. The number of elements can be reduced in the actuator since a motor, a temperature sensor and a power source are not necessary. In order to design the two-way SMA actuator using a bias spring, the graphical method is developed to evaluate the recovery force and recovery deflection in the SMA component [20]. If this approach is applied to the reciprocating rotary actuator by using torsional deformation of SMA tapes [9, 10], the design method of a simple rotary driving actuator can be developed.

In the present paper, the torsional deformation properties of TiNi SME tape showing SME and SE tape showing SE will be investigated in Section 2. Based on the torsional deformation properties of both tapes, the graphical method to design the bias-type reciprocating rotary driving actuator will be proposed in Section 3. The automatically opening and closing blind model driven by sun-

light will be demonstrated by using the reciprocating rotary driving element in Section 4.

2. Torsional deformation properties of SMA tapes

2.1. Materials and specimen

With respect to the SMAs, two kinds of polycrystalline TiNi alloy tapes showing the SME and SE at room temperature produced by Furukawa Techno Material Co., Ltd. were used. The SME tape showing the SME was a Ti-50.18at%Ni with a width of 5.9 mm and a thickness of 0.35 mm. The SE tape showing the SE at room temperature was a Ti-50.95at%Ni alloy tape with a width of 3.1 mm and a thickness of 0.66 mm. The temperatures A_f of the SME tape and SE tape obtained by the DSC test were 342 K and 291 K, respectively. The specimen was a uniform flat tape of a length of 70 mm. The gauge length L of the specimen was 40 mm and the length held by the grasping device was 15 mm at each end.

2.2. Experimental method

2.2.1. Experimental apparatus. In the previous study [7], the torsional load was controlled manually and the angle of twist was measured by using an angle measuring mark. Therefore, the torsional rate was not precisely prescribed and the angle of twist could not be measured exactly. In order to avoid these drawbacks, the torsion testing device in which both torque and angle of twist can be measured continuously was developed in the present study.

The photograph of the torsion testing device is shown in Fig. 1. The principle of driving part in the torsion testing device is shown in Fig. 2. The photograph of the torsion testing device mounted on the crosshead of the tension testing machine (Autograph AG-500, Shimadzu) is shown in Fig. 3. In the torsion testing

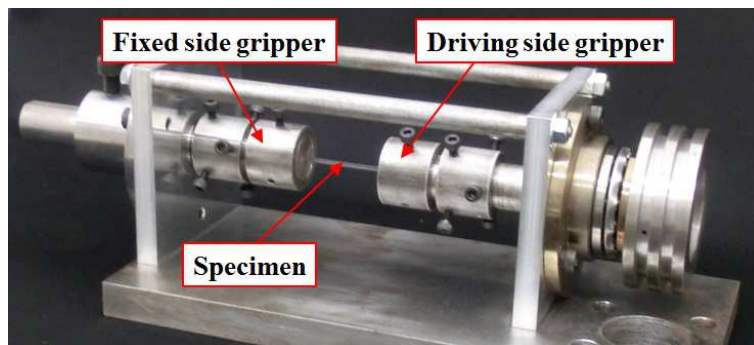


FIG. 1. Torsion testing device.

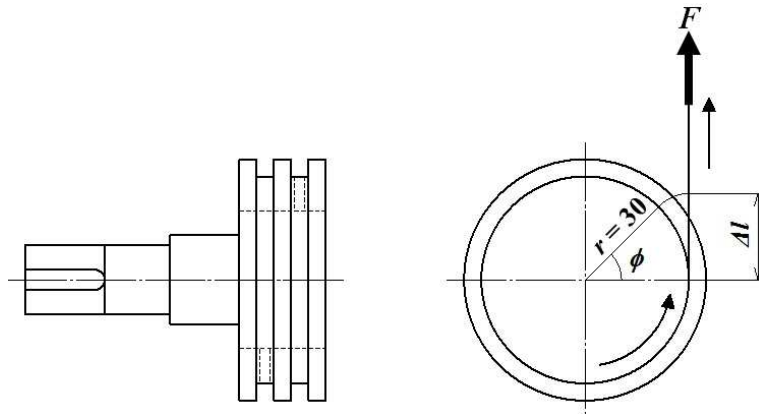


FIG. 2. Driving part in torsion testing device.



FIG. 3. Torsion testing device operated by tension tester.

machine, the specimen was mounted between the grippers. The left gripper was fixed and the right one was driven. The specimen was twisted by pulling the thin wire wound on the pulley, which was arranged horizontally to have the same shaft as the right driving gripper. The tensile load F and the displacement of the wire Δl were measured by the load-cell and the displacement of the crosshead in the tension testing machine, respectively. The displacement Δl expresses the circumferential displacement of the pulley. The torque $M = rF$ and the angle

of twist $\phi = \Delta l/r$ were obtained from F and Δl , where r was a radius of the pulley on which the wire was wound.

2.2.2. Experimental procedure. The specimen was twisted in the air under a constant torsional rate at the test temperature T . The torsional rate was controlled as follows. The displacement rate of the crosshead was 8 mm/s, which corresponds to the rate of twist angle per unit length θ of 6.5 rad/m/s. The angle of twist per unit length θ was obtained from the angle of twist ϕ and the gauge length L , as $\theta = \phi/L$. The maximum angle of twist per unit length θ_{\max} was 78.5 rad/m (maximum angle of twist $\phi_{\max} = \pi$ rad). The specimen was covered by a chamber and heated by using a heater. The test temperatures T for the SME tape were 293 K, 343 K and 373 K. The test temperature T for the SE tape was 293 K.

2.3. Torsional deformation

The relationships between torque M and angle of twist per unit length θ of the SME tape at various temperatures T are shown in Fig. 4. In SMAs, the plateau stress increases in proportion to temperature and torque therefore increases in proportion to temperature. At $T = 293$ K, a large residual angle of twist per unit length appears after unloading, which disappears by heating under no load, showing the SME. At $T = 343$ K, there appears a partial effect of superelasticity in which the reverse transformation does not completely occur, and therefore some residual angle of twist appears after unloading. At $T = 373$ K, the angle of twist recovers during unloading, showing the SE.

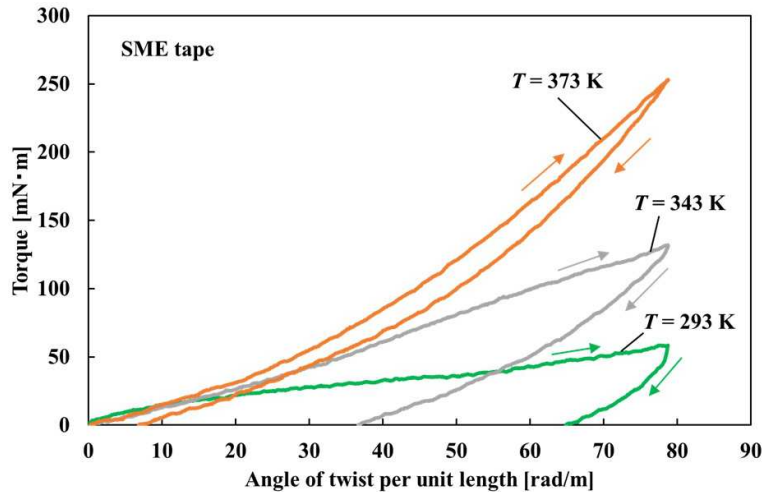


FIG. 4. Relationship between torque and angle of twist per unit length of SME tape at various temperatures T .

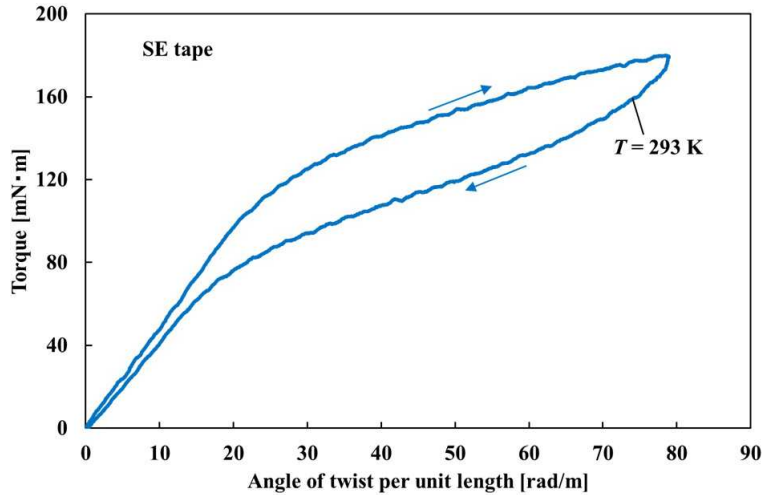


FIG. 5. Relationship between torque and angle of twist per unit length of SE tape at temperature $T = 293$ K.

The relationship between torque M and angle of twist per unit length θ of the SE tape at temperature $T = 293$ K is shown in Fig. 5. In the case of the SE tape, the angle of twist disappears during unloading, showing the SE at room temperature.

3. Design of bias-type reciprocating rotary actuator using SMA tapes

3.1. Reciprocating rotary element

The most widely used two-way element, which moves automatically by heating and cooling, is the bias-type. In practical components, the bias force is often provided by a spring since large deformation can be easily obtained. In the component, the SMA coil spring and another bias coil spring made of normal metal are arranged in series and the two coils mutually push against each other [19, 20]. At low temperatures, the SMA coil is pushed due to the bias force provided by the bias spring. If the temperature rises, the SMA coil pushes against the bias spring due to the recovery stress in the SMA coil. The action is two-way since the SMA coil will be pushed again when the temperature falls.

The principle of the reciprocating rotary element in which the torsional deformation of the SME tape and SE tape is used is shown in Fig. 6. The flat plane is shape-memorized in both SME tape and SE tape. Both tapes are arranged in series. The pretwisted SME tape is mounted with respect to the flat SE tape at low temperature. If the SME tape is heated, large recovery torque appears. The flat shape is therefore recovered in the SME tape and the SE tape is twisted.

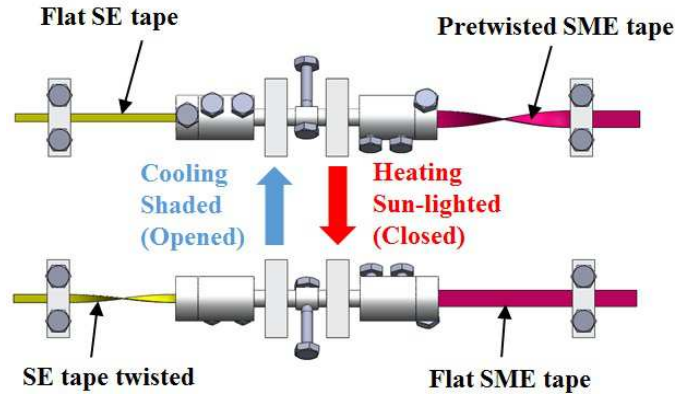


FIG. 6. Principle of driving actuation in bias-type reciprocating rotary element applied to solar-powered blind.

If the SME tape is cooled, recovery torque decreases and torque in the SE tape becomes higher. Then, the flat shape is recovered in the SE tape and the SME tape is twisted. Therefore, the driving part located between the two tapes is automatically twisted alternately in two directions by heating and cooling.

3.2. Design and control of reciprocating rotary actuator

The structure and principle of driving actuation of the driving part in the reciprocating rotary actuator was shown in Fig. 6. As shown in Fig. 6, both the SME tape pretwisted by an angle of π rad followed by unloading and the flat SE tape are mounted in series in the reciprocating rotary element. If the pretwisted SME tape is heated, the SME tape recovers its shape-memorized flat plane and therefore the SE tape is twisted. The recovery torque appears due to the reverse transformation during heating of the SME tape. Thus, in the case of two-way behavior, the torque due to the reverse transformation in the unloading process corresponds to the recovery torque [21]. By taking into account this property the loading curves at each temperature in the relationship between torque and angle of twist per unit length for the SME tape are presented by the dashed lines, and the unloading curves by the solid lines as shown in Fig. 7. In Fig. 7, point U ($\theta_r = 65.0$ rad/m) unloaded after twisting to point M ($\theta_{\max} = 78.5$ rad/m) at room temperature is taken at the origin on the loading curve of the SE tape as shown by the solid line (1). The driving element rotates from the point U to points H₁ and H₂ during heating in the direction of shape recovery of the SME tape. The torque increases due to the deformation resistance of the SE tape during the heating process of the SME tape. The torque generated in the SE tape increases from point U to points H₁ and H₂ corresponding to the heating

temperature T . Since the shape recovers due to the reverse transformation during heating of the SME tape, the torque generated at points H_1 and H_2 corresponds to the torque in the unloading process. As can be seen from the line (1), if the angle of twist per unit length is smaller than 20 rad/m, the SE tape remains in the elastic regime.

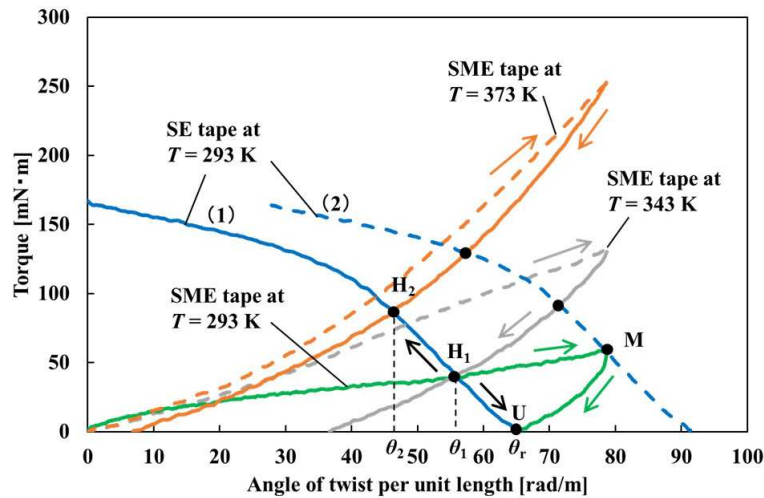


FIG. 7. Design chart of bias-type element in reciprocating rotary actuator.

Let us now consider the control of the reciprocating rotational angle of the SME tape. If the SME tape is mounted after unloading, the twisting angle is $\theta_r - \theta_2$ for the twisting angle θ_2 at the corresponding heating temperature T . If the SME tape is mounted with the state twisted at the angle θ_1 with the same torque as the SE tape, the twisting angle generated by heating is $\theta_1 - \theta_2$. One method to match the target twisting angle is to control θ_2 by adjusting the heating temperature T . Another method is to control θ_1 by adjusting the mounting angle. In the latter case, the SME tape is mounted at the maximum twisting point M and therefore the loading curve of the SE tape is drawn through point M as shown by the dashed line (2) in Fig. 7.

4. Automatically opening and closing blind driven by sunlight

4.1. Design of reciprocating rotary driving element for the blind

The bias-type reciprocating rotary element using the SME tape and SE tape is applied to the automatically opening and closing blind model driven by sunlight. The principle of the driving part in the reciprocating rotary element was explained in Fig. 6. The photograph of the driving part in the reciprocating

rotary element of solar-powered blind driven by the SME tape and SE tape is shown in Fig. 8. The flat SE tape and the pretwisted SME tape unloaded after twisting to an angle of π rad are mounted. As discussed in Section 3.2, the residual twisting angle and the twisting angle heated at temperature T are expressed by θ_r and $\theta(T)$, respectively. The original (opened) and sun-lighted (closed) states of the driving part and the blind part in the solar-powered blind are schematically shown in Figs. 9 and 10, respectively.



FIG. 8. Photograph of driving part in reciprocating rotary element of solar-powered blind.

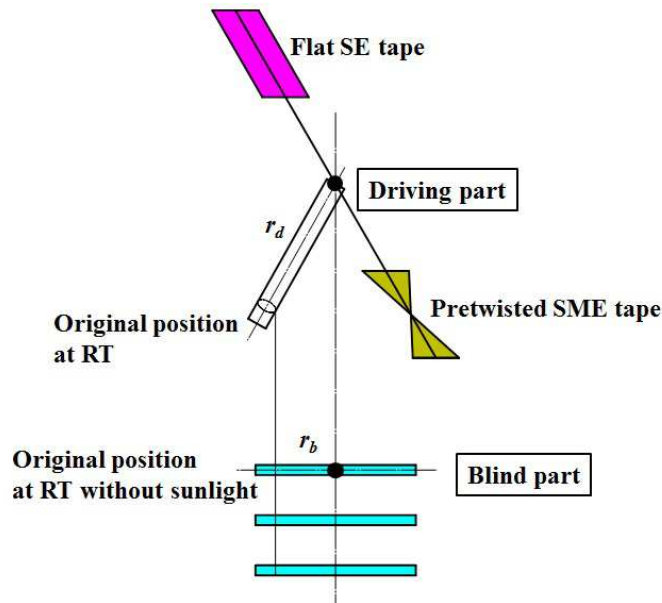


FIG. 9. Original opened state of driving part and blind part in solar-powered blind.

The rotational angle per unit length of the driving part θ_d , which is necessary to drive the SME tape and the SE tape, is as follows:

$$(4.1) \quad \theta_d = \theta_r - \theta(T).$$

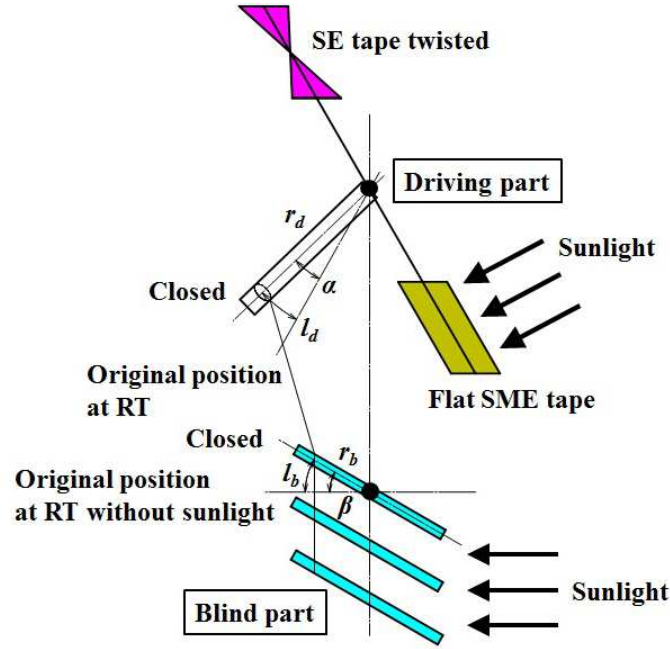


FIG. 10. Sun-lighted (closed) state of driving part and blind part in solar-powered blind.

The total rotational angle ϕ_d is

$$(4.2) \quad \phi_d = l\theta_d,$$

where l denotes the length between the grippers of each tape. The rotational angle of the driving part is expressed by α . The blind is opened or closed by the upward or downward motion of a wire. In this case, the twisting angle of the SME tape is equal to the rotational angle of the driving element, and therefore $\phi_d = \alpha$.

The distance between the center of the driving element and the tip where the wire is wound is denoted by r_d . The moving distance of the tip of the driving element l_d is expressed by the length of arc corresponding to the central angle α , and therefore

$$(4.3) \quad l_d = r_d\alpha.$$

The driving element and the blind are connected by the wire. The distance between the rotation center of the blind and the tip where the wire is wound is expressed by r_b . The rotational angle of the blind is denoted by β . The moving distance of the tip of the blind l_b is expressed by the length of arc corresponding to the rotational angle β , and therefore

$$(4.4) \quad l_b = r_b\beta.$$

In the case of $r_d = r_b$, since the moving distance of the blind l_b is caused by the moving distance of the driving element l_d , $l_b = l_d$, and therefore $\alpha = \beta$.

The rotational angle of the blind β was measured at the prescribed temperature of the SME tape heated by a heater. The rotational angle per unit length θ_d of the SME tape was obtained from Eq. (4.2). The relationship between the rotational angle per unit length θ_d and temperature obtained during heating and cooling is shown by the dashed line in Fig. 11. The rotational angle obtained by using the design chart shown in Fig. 7 is expressed by the solid line. As can be seen, the movement of the blind during heating can be well estimated by the proposed design method. However, there exists the angle-lag in the movement of the blind during cooling. The hysteresis of the rotational angle corresponds to the behavior of the recovery stress. The recovery stress increases in the reverse transformation band located at higher temperature region on the stress-temperature phase diagram during heating and decreases in the forward transformation band located at lower temperature region during cooling [21]. That is, the reverse transformation during heating appears at higher temperature and the forward one during cooling at lower temperature. The hysteresis of the angle of twist during heating and cooling, therefore, appears due to the difference in temperature between the reverse and forward transformations.

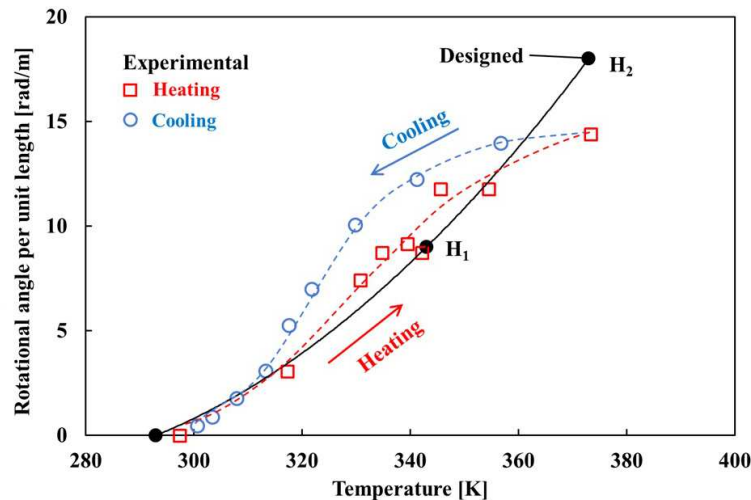


FIG. 11. Relationship between rotational angle per unit length and temperature in rotary element.

4.2. Blind model driven by sunlight

The blind model using torsional deformation of the SME tape and SE tape driven by sunlight was produced. The photograph of the solar-powered blind is

shown in Fig. 12. The principle of the driving actuation and the photograph of the driving part were shown in Figs. 6 and 8, respectively. The photographs of the opened and closed states of the blind are shown in Fig. 13.

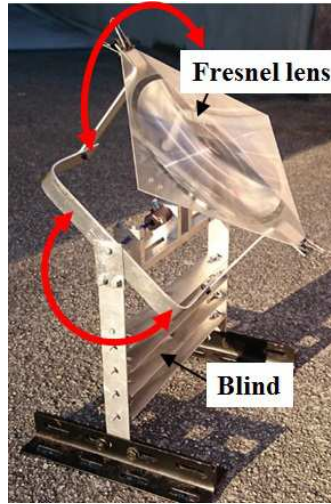


FIG. 12. Photograph of solar-powered blind.

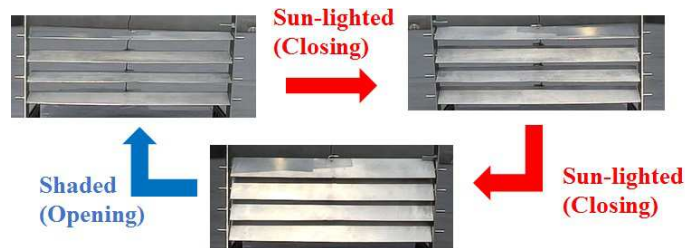


FIG. 13. Photographs of opened and closed states of solar-powered blind.

The SME tape is heated by the sunlight passing through a Fresnel lens. The Fresnel lens can be rotated around the axis of the driving part with the SME and SE tapes and around the direction normal to the axis as shown by the arrows in Fig. 12. The Fresnel lens can therefore be moved to concentrate sunlight onto the SME tape if the position of the sun moves. If the sunlight is focused on the SME tape, the temperature of the SME tape can rise up to 473 K.

In the model, $r_d = r_b = 20$ mm, and therefore $\alpha = \beta$ as explained in Section 4.1. The sunlight can be blocked by the rotational angle of the blind $\beta = \pi/4$ rad from the horizontal direction. Since $r_b = 20$ mm, $l_b = r_b\beta = 15.7$ mm.

The distance between grippers is 40 mm. If the twisting angle per unit length $\theta_d = \alpha/l$ varies by 19.6 rad/m, the total twisting angle $\phi_d = l\theta_d$ is 0.78 rad from Eq. (4.2). Hence the moving distance of the tip of the driving element $l_d = r_d\alpha = 15.7$ mm, and the blind thereby closes.

The opening and closing behavior of the blind was demonstrated in Fig. 13. The blind is opened in the sunlight and closed in the shade. The cyclic deformation and fatigue properties, the scales and the MT temperatures of the SME tape and SE tape, and the focal length to obtain the appropriate temperature on the surface of the SMA tape are the subjects of future studies.

5. Conclusions

In order to develop the reciprocating rotary driving actuator using SMA tapes, the graphical method to design the actuator was proposed based on the torsional deformation properties of the SME tape and the SE tape. The blind model using the reciprocating rotary element driven by sunlight was demonstrated. The results obtained are summarized as follows.

1. The torsional deformation properties of the SME tape and the SE tape were obtained. The reciprocating rotary actuator was composed of the pretwisted SME tape and the flat SE tape in series. Based on the torsional deformation properties, the design chart expressed by the relationship between torque and twisting angle of the SME tape and the SE tape was proposed. The rotational angle and torque, which vary depending on temperature, can be estimated based on the design chart. The rotational angle is controlled by adjusting the mounting angle of the SME tape and the heating temperature. It is noted that there exists the hysteresis of the rotational angle due to the reverse and forward transformations during heating and cooling, respectively. The behavior of the reciprocating rotary actuator with a simple mechanism can be obtained by the proposed design method.

2. The automatically opening and closing blind driven by sunlight was demonstrated. The blind was controlled by using the reciprocating rotary element composed of the SME tape and the SE tape. In the reciprocating rotary element, the SME tape was heated by the sunlight passing through the Fresnel lens. The blind is opened in the sunlight and closed in the shade. The behavior of the blind can be achieved based on the proposed design method of the reciprocating rotary driving element.

Acknowledgement

The experimental work for this study was carried out with the assistance of students in Aichi Institute of Technology, to whom the authors wish to express

their gratitude. The authors also wish to extend thanks to the administrators of Scientific Research (C) (General) in Grants-in-Aid for Scientific Research by the Japan Society for Promotion of Science for financial support.

References

1. H. FUNAKUBO [Ed.], *Shape Memory Alloys*, Gordon and Breach Science Pub., 1–60, 1987.
2. T.W. DUERIG, K.N. MELTON, D. STOCKEL, C.M. WAYMAN [Eds.], *Engineering Aspects of Shape Memory Alloys*, Butterworth-Heinemann, 1–35, 1990.
3. K. OTSUKA, C.M. YAYMAN, *Shape Memory Materials*, Cambridge University Press, 1–49, 1998.
4. H. TOBUSHI, R. MATSUI, K. TAKEDA, E.A. PIECZYSKA, *Mechanical Properties of Shape Memory Materials*, Nova Science Pub., 1–103, 2013.
5. J.H. MABE, R.T. RUGGERI, E. ROSENZWEIG, C.J. YU, *Nitinol performance characterization and rotary actuator design*, Smart Struct. Mater.: 2004, Proc. of SPIE, **5388**, 95–109, 2004.
6. J.H. MABE, F.T. CALKINS, R.T. RUGGERI, *Full-scale flight tests of aircraft morphing structures using SMA actuators*, Proc. of SPIE, 6525–65251C, 1–12, 2007.
7. H. TOBUSHI, E.A. PIECZYSKA, W.K. NOWACKI, T. SAKURAGI, Y. SUGIMOTO, *Torsional deformation and rotary driving characteristics of SMA thin strip*, Arch. Mech., **61**, 3–4, 241–257, 2009.
8. E. PIECZYSKA, H. TOBUSHI, K. DATE, K. MIYAMOTO, *Torsional deformation and fatigue properties of TiNi SMA thin strip for rotary driving element*, J. Solid Mech. Mater. Eng., **4**, 8, 1306–1314, 2010.
9. H. TOBUSHI, E.A. PIECZYSKA, W.K. NOWACKI, K. DATE, K. MIYAMOYO, *Two-way rotary shape memory alloy thin strip actuator*, J. Theo. Appl. Mech., **48**, 4, 1043–1056, 2010.
10. H. TOBUSHI, E. PIECZYSKA, K. MIYAMOTO, K. MITSUI, *Shape-memory alloy thin strip rotary actuator*, Mater. Sci. Forum, **674**, 219–224, 2011.
11. H. FUNAKUBO [Ed.], *Shape Memory Alloys*, Gordon and Breach Science Pub., 33–36, 1987.
12. A. OUDICH, F. THIEBAUD, *A two-way shape memory alloy-piezoelectric bimorph for thermal energy harvesting*, Mech. Mater., **102**, 1–6, 2016.
13. A. NESPOLI, S. BESSEGHINI, S. PITTACCIO, E. VILLA, S. VISCUSO, *The high potential of shape memory alloys in developing miniature mechanical devices: A review on shape memory alloy mini-actuators*, Sens. Actuators A Phys., **158**, 149–160, 2010.
14. A. NESPOLI, E. BASSANI, S. BESSEGHINI, E. VILLA, *Rotational mini-actuator activated by two antagonist shape memory alloy wires*, Phys. Procedia, **10**, 182–188, 2010.
15. X.Y. ZHANG, X.J. YAN, *Continuous rotary motor actuated by multiple segments of shape memory alloy wires*, J. Mater. Eng. Perform., **21**, 2643–2649, 2012.

16. O. BENAFAN, J. BROWN, F.T. CALKINS, P. KUMAR, A.P. STEBNER, T.L. TURNER, R. VAIDYANATHAN, J. WEBSER, M.L. YOUNG, *Shape memory alloy actuator design: CAS-MART collaborative best practices and case studies*, Int. J. Mater. Des., **10**, 1–42, 2014.
17. Z. GUO, Y. PAN, L.B. WEE, H. YU, *Design and control of a novel compliant differential shape memory alloy actuator*, Sens. Actuators A Phys., **225**, 71–80, 2015.
18. K. SAITO, K. IWATA, Y. ISHIHARA, K. SUGITA, M. TAKATO, F. UCHIKOBA, *Miniaturized rotary actuators using shape memory alloy for insect-type MEMS microrobot*, Micromachines, **7**, 4, 58, 2016; doi: 10.3390/mi7040058.
19. T.W. DUERIG, K.N. MELTON, D. STOCKEL, C.M. WAYMAN [Eds.], *Engineering Aspects of Shape Memory Alloys*, Butterworth-Heinemann, 245–266, 1990.
20. H. FUNAKUBO [Ed.], *Shape Memory Alloys*, Gordon and Breach Science Pub., 177–194, 1987.
21. P.H. LIN, H. TOBUSHI, K. TANAKA, C. LEXCELLENT, A. IKAI, *Recovery stress of TiNi shape memory alloy under constant strain*, Arch. Mech., **47**, 2, 281–293, 1995.

Received October 13, 2016; revised version December 23, 2016.
